Raman scattering spectra and ferroelectric properties of $Bi_{1-x}Nd_xFeO_3$ ($x=0-0.2$) multiferroic ceramics

G. L. Yuan, Siu Wing Or,[a] and Helen Lai Wa Chan
Department of Applied Physics, The Hong Kong Polytechnic University, Hung Hom, Kowloon, Hong Kong

(Received 14 July 2006; accepted 29 November 2006; published online 16 March 2007)

Single-phase $Bi_{1-x}Nd_xFeO_3$ ($BNFO_x$) ($x=0-0.2$) multiferroic ceramics were prepared to study the effects of Nd substitution on their crystal structures, Raman scattering spectra, and ferroelectric properties. Rietveld refinement of x-ray diffraction data showed a gradual change in crystal structure from rhombohedral to pseudotetragonal via triclinic with increasing x. The evolvement of Raman normal modes with increasing x suggested that such structural change is accompanied by the weakening of long-range ferroelectric order. The simultaneous occurrence of abrupt mode evolvement and ferroelectric-paraelectric transition in $BNFO_{x=0.175}$ and $BNFO_{x=0.2}$ was explained according to the change of Bi–O covalent bonds as a result of the decline in the stereochemical activity of the Bi lone electron pair at $0.175 \leqslant x \leqslant 0.2$. © *2007 American Institute of Physics*. [DOI: 10.1063/1.2433709]

I. INTRODUCTION

Single-phase $BiFeO_3$, which shows ferroelectric order below a high Curie temperature ($T_{C\text{-FE}}$) of ~830 °C and G-type canted antiferromagnetic order below a high Néel temperature ($T_{N\text{-AFM}}$) of ~370 °C, is an important multiferroic material.[1,2] It is known that single-phase bulk $BiFeO_3$ has a rhombohedral symmetry with the space group $R3c$.[1] Its ferroelectric order originates from the stereochemical activity of the Bi lone electron pair.[1,2] In more detail, as the A-site Bi^{3+} ion of $BiFeO_3$ shows a valence electron configuration of $6s^26p^0$, the lone $6s^2$ electrons of Bi^{3+} ion hybridize with both the empty $6p^0$ orbits of Bi^{3+} ion and the $2p^6$ electrons of O^{2-} ion to form Bi–O covalent bonds, leading to a structural distortion and hence ferroelectric order.[1,3,4] This is characterized by the second-order Jahn-Teller effect and, in this case, is referred to the stereochemical activity of the Bi lone electron pair. In contrast with $BiFeO_3$ ceramic, the B-site cation-oxygen covalency is the principal driving force of ferroelectric order in conventional perovskite oxide ferroelectrics.[1,3,4] On the other hand, the G-type canted antiferromagnetic order in $BiFeO_3$ is mainly attributed to the first-order Jahn-Teller (structural) distortion controlled by the partially filled $3d$ orbits of the B-site Fe^{3+} ion.[1,3,4] In fact, this G-type canted antiferromagnetic order is not homogenous in space; it has an incommensurately space-modulated spin structure along the $(110)_h$ direction with a long wavelength of 620 Å instead.[5–7] As a result, the possible nonzero remnant magnetization (M_r) permitted by the G-type canted antiferromagnetic order is canceled by the space-modulated spin structure, significantly restricting the release and measurement of weak ferromagnetism.[5–8]

By substituting rare-earth cations (e.g., La^{3+}, Nd^{3+}, or Sm^{3+} ion) for the A-site Bi^{3+} ion in the nominal $BiFeO_3$ composition, it can effectively modulate the crystal structure parameters of $BiFeO_3$, destroy the space-modulated spin structure, and release the measurement of weak ferromagnetism.[6,9–12] It is only quite recently that the coexistent effects of ferroelectricity, piezoelectricity, and weak ferromagnetism were realized in single-phase bulk $Bi_{1-x}Nd_xFeO_3$ ($BNFO_x$) ($x=0.15-0.175$) system.[11,12] However, too much Nd substitution led to weakening the stereochemical activity of the Bi lone electron pair and thus inducing the ferroelectric-paraelectric (FE-PE) transition since ferroelectricity of such Nd-substituted $BiFeO_3$ comes from the described stereochemical activity.[1,3,4]

Since spontaneous polarization is closely related to atomic displacements, Raman scattering is an effective technique to explore the dependence of crystal structure parameters on Raman scattering spectra, to clarify the relationships between the Raman normal modes, the ferroelectric order, and the corresponding chemical bonds, as well as to explain the origin of the FE-PE transition. Besides, the weak ferromagnetic trait of multiferroic materials can also affect the Raman scattering spectra through some other relatively weak second-order effects (e.g., spin-phonon coupling).[13] In spite of their importance, Raman scattering study of single-phase $BiFeO_3$-based materials, bulk $BNFO_x$ especially, has not been reported due to the well-known difficulty in assigning normal modes.[14–16] Recently, Singh *et al.* have assigned most of the normal modes of the $(111)_c$-oriented $BiFeO_3$ epitaxial films with rhombohedral $R3c$ symmetry and the $(001)_c$-oriented $BiFeO_3$ epitaxial films with pseudotetragonal symmetry.[17,18] In this paper, we decompose the dynamic ferroelectric modes of $Bi_{1-x}Nd_xFeO_3$ ($BNFO_x$) ($x=0-0.2$) (where $BNFO_{x=0}$ is $BiFeO_3$) and explore the relationships among the Raman scattering spectra, FE-PE transition, Bi–O covalent bonds, and stereochemical activity of the Bi lone electron pair.

II. EXPERIMENTAL DETAILS

The specific synthesis technique that was demonstrated in our recent studies in preparing single-phase bulk $BNFO_{x=0-0.15}$ ceramics was used in the present study to pre-

[a]Author to whom correspondence should be addressed; electronic mail: apswor@polyu.edu.hk

 © 2007 American Institute of Physics

Downloaded 10 Feb 2009 to 158.132.12.80. Redistribution subject to AIP license or copyright; see http://jap.aip.org/jap/copyright.jsp

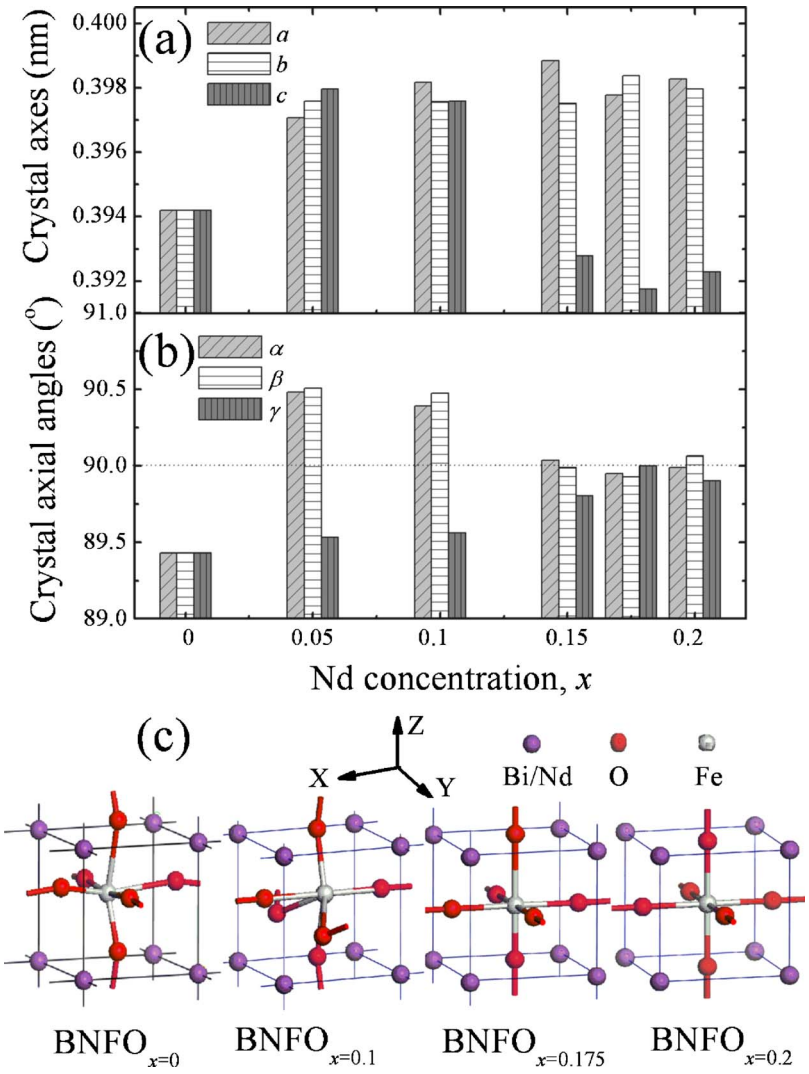

FIG. 1. (Color online) Refined (a) crystal axes, (b) crystal axial angles, and (c) unit cells of $BNFO_{x=0-0.2}$ samples.

pare disk-shaped $BNFO_{x=0-0.2}$ samples with a diameter of 5 mm and thickness of 1 mm.[11] This technique involved the use of high-purity (>99%) Bi_2O_3, Fe_2O_3, and Nd_2O_3 powders of <1 μm size and a rapid liquid-phase sintering process of 855 °C for 20 min at a heating rate of >100 °C/s and a cooling rate of >10 °C/s. It is noted that the adoption of such a rapid liquid-phase sintering process is essentially different from the slow heating and cooling rates combined with a long sintering time engaged in the conventional sintering process. Further details about the synthesis technique can be found elsewhere.[9–12]

The crystal structure of the sintered samples was examined by an x-ray diffractometer (Brucker D8 Advance System) with a 2θ step size of 0.02° and at a scan rate of one step every 4 s. Simulation of crystal structure based on the measured x-ray diffraction (XRD) data was carried out using a Rietveld crystal structure refinement software (FULLPROF 2000). Raman scattering spectra were measured at room temperature using a Raman spectrometer (SPEX 1403) in backscattering geometry. The excitation source was the 514.5 nm line of an Ar^+ laser with 200 mW output. The power of the laser spot on the sample was less than 20 mW so that sample heating was insignificant. The data were collected with each increment of 0.6 cm^{-1} and an integration time of 1 s. The samples were then thinned down to 0.4 mm thick, and silver paste was applied on their two major surfaces as electrodes for subsequent measurements. The polarization hysteresis (*P-E*) loops at room temperature were measured with a ferroelectric tester (Radiant RT6000-HVS).

III. RESULTS AND DISCUSSION

A. Crystal structures

The measured XRD patterns of $BNFO_{x=0-0.2}$ samples were simulated according to the initial conditions of triclinic symmetry, *P*1 space group, and a single unit cell with *A*-site Bi/Nd mixed atoms.[10,12] The simulated XRD patterns were found to coincide well with the measured XRD patterns in terms of generally small *R* values (i.e., $\leqslant$8.84% for R_{wp} and $\leqslant$6.32% for R_p). Hence, we present the exact crystal axes, crystal axial angles, and simulated unit cells of the samples in Fig. 1.

For $BNFO_{x=0}$ sample, it is clear that both the refined crystal axes ($a=b=c=0.3942$ nm) [Fig. 1(a)] and crystal axial angles ($\alpha=\beta=\gamma=89.43°$) [Fig. 1(b)] are consistent with rhombohedral *R*3*c* symmetry.[9,10] With increasing Nd

Downloaded 10 Feb 2009 to 158.132.12.80. Redistribution subject to AIP license or copyright; see http://jap.aip.org/jap/copyright.jsp

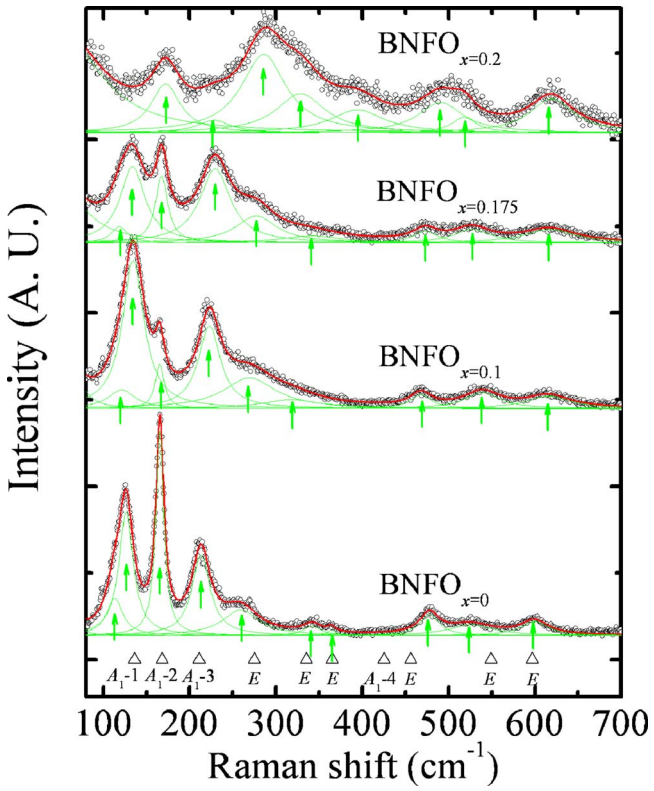

FIG. 2. (Color online) Measured Raman scattering spectra (open circles), together with their fitted spectra (thick solid line) and the decomposed active modes (thin solid lines and arrows), for BNFO$_{x=0}$, BNFO$_{x=0.1}$, BNFO$_{x=0.175}$, and BNFO$_{x=0.2}$ samples at room temperature. The ten normal modes of the $(111)_c$-oriented $BiFeO_3$ epitaxial thin film with rhombohedral $R3c$ symmetry (open triangles and labels) are extracted from Ref. 17 for comparison with BNFO$_{x=0}$ sample.

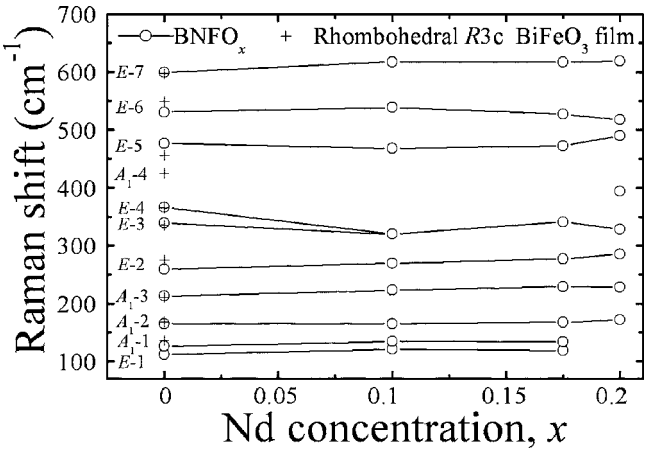

FIG. 3. Raman mode frequency associated with each of the decomposed active modes in Fig. 2 as a function of Nd concentration x for BNFO$_{x=0}$, BNFO$_{x=0.1}$, BNFO$_{x=0.175}$, and BNFO$_{x=0.2}$ samples. The Raman mode frequencies associated with the ten normal modes of the $(111)_c$-oriented $BiFeO_3$ epitaxial thin film with rhombohedral $R3c$ symmetry are extracted from Ref. 17 for comparison with BNFO$_{x=0}$ sample.

concentration x, distortions of crystal structure from rhombohedral $R3c$ symmetry of BNFO$_{x=0}$ to triclinic $P1$ symmetry (i.e., $a \neq b \neq c$; $\alpha \approx \beta > \gamma$) occur in BNFO$_{x=0.05}$, BNFO$_{x=0.1}$, and BNFO$_{x=0.15}$. Both BNFO$_{x=0.175}$ and BNFO$_{x=0.2}$ exhibit pseudotetragonal symmetry (i.e., $a \approx b > c$ and $\alpha \approx \beta \approx \gamma \approx 90°$). In particular, BNFO$_{x=0.175}$ should have pseudotetragonal $P4mm$ symmetry due to its noncentrosymmetric ferroelectricity, and BNFO$_{x=0.2}$ should have pseudotetragonal $P4/mmm$ symmetry because of its centrosymmetric paraelectricity.[12] Figure 1(c) shows the simulated unit cells where Bi^{3+} ion is designated as the origin of the coordinate at (0, 0, 0). It is seen that Fe^{3+} ion of BNFO$_{x=0}$ at (0.5967, 0.5046, 0.5724) and that of BNFO$_{x=0.1}$ at (0.4383, 0.4617, 0.5677) distort significantly from the center position of unit cell at (0.5, 0.5, 0.5). For BNFO$_{x=0.175}$, Fe^{3+} ion at (0.5, 0.5, 0.4875) distorts slightly from (0.5, 0.5, 0.5) along the $(0,0,1)_c$ axis. For BNFO$_{x=0.2}$, Fe^{3+} ion centers at (0.5, 0.5, 0.5) owing to its centrosymmetric paraelectricity. This structural change always accompanies the change of Bi–O covalent bonds, including the bond length and the bond angle. As expected, the continuing change in crystal structure parameters of BNFO$_{x=0-0.2}$ gives rise to the continuing collapse of the space-modulated spin structure, which was confirmed by the continuing increase in M_r with increasing x (e.g., M_r of 0.07–0.227 emu/g in BNFO$_{x=0.15-0.2}$).[9]

B. Raman scattering spectra

Figure 2 shows the measured Raman scattering spectra of BNFO$_{x=0}$, BNFO$_{x=0.1}$, BNFO$_{x=0.175}$, and BNFO$_{x=0.2}$ samples at room temperature. By fitting the measured spectra and decomposing the fitted curves into individual Lorentzian components, the peak position of each component, i.e., the natural frequency (cm^{-1}) of each Raman active mode, was obtained in the samples. Then, these mode frequencies are plotted as a function of Nd concentration x in Fig. 3.

It has been reported that the Raman active modes of the rhombohedral $R3c$ $BiFeO_3$ can be summarized using the following irreducible representation: $\Gamma = 4A_1 + 9E$.[13,17,19] For $(111)_c$-oriented $BiFeO_3$ epitaxial films with rhombohedral $R3c$ symmetry, there are ten normal modes, including A_1-1, A_1-2, and A_1-3 modes with strong scattering intensities at 136, 168, and 211 cm^{-1}, respectively, A_1-4 mode with quite weak scattering intensity at 425 cm^{-1}, and six E modes with medium scattering intensities at 275, 335, 365, 456, 549, and 597 cm^{-1}.[17] These ten normal modes are also included in Figs. 2 and 3 for comparison with our decomposed active modes of the BNFO$_{x=0}$ sample. It is obvious that the normal modes of the $(111)_c$-oriented $BiFeO_3$ epitaxial films agree well with the decomposed active modes of our BNFO$_{x=0}$ sample in terms of relative scattering intensity (Fig. 2) and mode frequency (Figs. 2 and 3). These agreements suggest the viability of assigning the decomposed active modes of our BNFO$_{x=0}$ sample based on the ten normal modes of the $(111)_c$-oriented $BiFeO_3$ epitaxial films.[17] From Figs. 2 and 3, the first three strong peaks at 126.1, 165.5, and 213.0 cm^{-1} manifest A_1-1, A_1-2, and A_1-3 modes, respectively, even though A_1-4 mode at ~425 cm^{-1} is very weak to be accurately decomposed. Nevertheless, there is a negligible splitting between longitudinal-optical A_1 and transverse-optical A_1 modes in our sample due to the domination of the short-range interatomic force compared to the long-range ionic force reported in the rhombohedral $R3c$ $BiFeO_3$ epitaxial films.[17] A small peak at 111.7 cm^{-1} should be assigned as E-1 mode, and the remaining six small peaks at 259.5, 339.6, 366.6, 476.9, 530.9, and 599.6 cm^{-1} are assigned to be E-2, E-3, E-4, E-5, E-6, and E-7 modes (where the number is

Downloaded 10 Feb 2009 to 158.132.12.80. Redistribution subject to AIP license or copyright; see http://jap.aip.org/jap/copyright.jsp

only named for convenience), respectively, because of their good agreements with the six E modes found in the rhombohedral $R3c$ $BiFeO_3$ epitaxial films.[17] Since the effects of internal stress and possible oxygen vacancy in our $BNFO_{x=0}$ sample have been reduced in comparison with those in the rhombohedral $R3c$ $BiFeO_3$ epitaxial films, the mode frequency of A_1-1, E-2, and E-6 softens to 126.1, 259.5, and 530.9 cm^{-1}, respectively, while that of E-5 hardens to 476.9 cm^{-1} in our $BNFO_{x=0}$ sample.[17]

Since Raman scattering spectra are sensitive to atomic displacements, the evolvement of Raman normal modes with increasing x can provide valuable information about ionic substitution and electric polarization. In our $BNFO_{x=0–0.175}$ samples (Figs. 2 and 3), E-1, A_1-1, A_1-2, A_1-3, and E-2 modes at 111.7, 126.1, 165.5, 213.0, and 259.5 cm^{-1}, respectively, should be dominated by the Bi–O covalent bonds according to the following two main facts. First, these five characteristic modes have been found to coincide well with those of the rhombohedral $R3c$ $BiFeO_3$ epitaxial films in the previous paragraph.[17] Second, they are also found to concur with those at ~126, 136, 168, 212, and 257 cm^{-1}, respectively, in the pseudotetragonal $P4mm$ $BiFeO_3$ epitaxial films.[18] Indeed, the Bi–O covalent bonds have been proven to dominate these five modes in the pseudotetragonal $P4mm$ $BiFeO_3$ epitaxial films.[18] Therefore, the good agreement on these five characteristic modes obtained in our $BNFO_{x=0–0.175}$ samples, the rhombohedral $R3c$ $BiFeO_3$ epitaxial films, and the pseudotetragonal $P4mm$ $BiFeO_3$ epitaxial films is likely due to the common origin of ferroelectric order. This means that the stereochemical activity of the Bi lone electron pair plays the main role in the change of both Bi–O covalent bonds and five characteristic modes, although the crystal symmetry varies from rhombohedral $R3c$ symmetry to pseudotetragonal $P4mm$ symmetry in the $BiFeO_3$ epitaxial films and, for our samples, from rhombohedral $R3c$ symmetry in $BNFO_{x=0}$ to triclinic $P1$ symmetry in $BNFO_{x=0.05–0.15}$ and finally to pseudotetragonal $P4mm$ symmetry in $BNFO_{x=0.175–0.2}$. These physical sources can provide an effective explanation for the following phenomena associated with the Raman scattering spectra in Figs. 2 and 3.

(1) With increasing x, there is a change of Bi–O covalent bonds as a result of the decline in the stereochemical activity of the Bi lone electron pair and thus in long-range ferroelectric order. This change, in conjunction with the A-site ion disorder induced by the Nd substitution, weakens the intensity and broadens the width of almost all normal modes. In fact, the presence of the A-site ion disorder commonly brings a continuous and slow change for mode intensity. Thus, the faster change of Bi–O covalent bonds near the FE-PE transition leads to a faster drop in mode intensity. In Fig. 2, as the threefold intensity of E-1, A_1-1, A_1-2, and A_1-3 modes in $BNFO_{x=0.2}$ is still smaller than the intensity of these modes in $BNFO_{x=0.175}$, the faster drop in intensity of E-1, A_1-1, A_1-2, and A_1-3 modes from $BNFO_{x=0.175}$ to $BNFO_{x=0.2}$ should be regarded as the change of Bi–O covalent bonds near the FE-PE transition. That is to say, the stereochemical activity of the Bi lone electron pair is too weak to result in ferroelectric order so that the corresponding modes weaken abruptly in $BNFO_{x=0.2}$.[9]

(2) E-1, A_1-1, A_1-2, A_1-3, and E-2 modes shift gradually to higher mode frequencies with increasing x. These modes are governed by the Bi–O covalent bonds. If mode frequency is governed by local factors, such as the force constant and ionic mass of the substitutive elements as well, it will be proportional to $(k/M)^{1/2}$, where k is the force constant and M is the reduced mass.[20] Since the valence and ionic radius of Nd^{3+} ion are similar to those of Bi^{3+} ion, k is assumed to be independent of the substitution as a zero approximation. However, as the mass of Nd^{3+} ion is 31% less than that of Bi^{3+} ion, the relatively light Nd^{3+} ion may cause an increase in mode frequency.

(3) E-1 and A_1-1 modes disappear in the $BNFO_{x=0.2}$ sample but present in the $BNFO_{x=0.175}$ sample. When x is increased from 0.175 to 0.2, the stereochemical activity of the Bi lone electron pair may undergo an abrupt drop so that the corresponding discrete Bi–O covalent bonds may change to a degeneracy state and finally are unable to cause a structural distortion and an introduction of ferroelectricity at $x=0.2$.[3,4,9] The change of crystal structure and Bi–O covalent bonds can be observed in Fig. 1(c). Since E-1 and A_1-1 modes are governed by the Bi–O covalent bonds which are the origin of ferroelectric order, the change of Bi–O covalent bonds is essentially due to the disappearance of E-1 and A_1-1 modes in $BNFO_{x=0.2}$.

(4) A mode at 394.2 cm^{-1} is observed in $BNFO_{x=0.2}$ sample. The observed mode is consistent with the expected A_1-4 mode of the rhombohedral $R3c$ $BiFeO_3$ epitaxial films.[17] This mode cannot be decomposed for x varying from 0 to 0.175 due to its low scattering intensity. With $x=0.2$, the strong peaks of A_1-1, A_1-2, and A_1-3 disappear or weaken abruptly, leading to the enhancement of A_1-4 mode. Also, it becomes decomposable in $BNFO_{x=0.2}$.

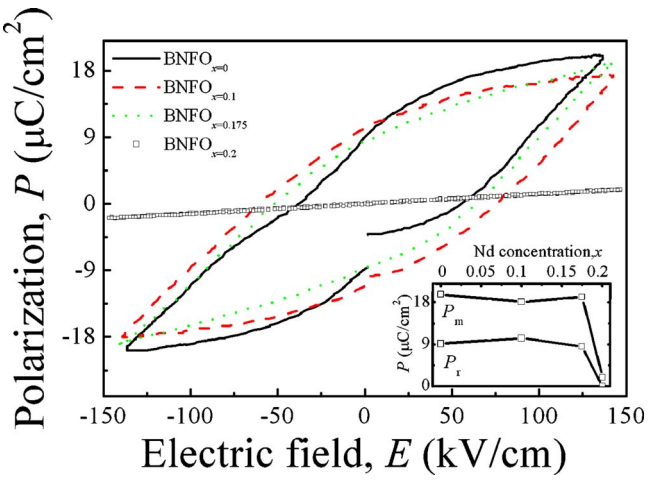

FIG. 4. (Color online) Polarization hysteresis (P-E) loops of $BNFO_{x=0}$, $BNFO_{x=0.1}$, $BNFO_{x=0.175}$, and $BNFO_{x=0.2}$ samples at room temperature. The inset shows the dependence of the maximum polarization (P_m) and remnant polarization (P_r) of the samples as a function of Nd concentration x.

C. Ferroelectric properties

Figure 4 shows the polarization hysteresis (P-E) loops of

Downloaded 10 Feb 2009 to 158.132.12.80. Redistribution subject to AIP license or copyright; see http://jap.aip.org/jap/copyright.jsp

$BNFO_{x=0}$, $BNFO_{x=0.1}$, $BNFO_{x=0.175}$, and $BNFO_{x=0.2}$ samples at room temperature. The inset plots the dependence of the maximum polarization (P_m) and remnant polarization (P_r) of the samples as a function of Nd concentration x. Obvious ferroelectric behaviors with P_m of $\sim 19\ \mu C/cm^2$ and P_r of $\sim 9\ \mu C/cm^2$ are observed in the $BNFO_{x=0}$, $BNFO_{x=0.1}$, and $BNFO_{x=0.175}$ samples, whereas paraelectric behaviors with P_m of $1.9\ \mu C/cm^2$ and P_r of $\sim 0\ \mu C/cm^2$ are seen in the $BNFO_{x=0.2}$ sample.[9] Although Bi^{3+} ion has been partially substituted by Nd^{3+} ion, the stereochemical activity of the Bi lone electron pair still results in the noncentrosymmetric ferroelectric order in our $BNFO_{x=0-0.175}$ samples.[1,3,4] At $x=0.175-0.2$, the abrupt drop in P_r confirms the FE-PE transition that can be explained by the evolvement of the stereochemical activity of the Bi lone electron pair and the change of Bi–O covalent bonds. Accompanied with this FE-PE transition, the relative displacement between Fe^{3+} ion and the charge center of O^{2-} octahedron along the $(001)_c$ axis in the pseudotetragonal $P4mm$ $BNFO_{x=0.175}$ disappears, leading to centrosymmetric pseudotetragonal $P4/mmm$ symmetry in our $BNFO_{x=0.2}$ sample.

IV. CONCLUSION

The crystal structure, ferroelectric order, Raman normal modes, and the corresponding chemical bonds (especially the Bi–O covalent bonds) have been discussed in single-phase bulk $BNFO_{x=0-0.2}$ multiferroic ceramics. The A-site substitution of Nd^{3+} ion has shown to weaken the stereochemical activity of the Bi lone electronic pair, to induce a change of Bi–O covalent bonds, to decrease the Raman scattering intensity, to broaden the width of normal modes, to increase the mode frequency at $x=0-0.175$, and to induce the FE-PE transition accompanied by the abrupt change of Raman scattering spectra at $x=0.175-0.2$.

ACKNOWLEDGMENT

This work was supported by the Research Grants Council of the HKSAR Government under Grant Nos. PolyU 5255/03E and PolyU 5122/05E.

[1] M. Fiebig, J. Phys. D **38**, R123 (2005).
[2] W. Eerenstein, N. D. Mathur, and J. F. Scott, Nature (London) **442**, 579 (2006).
[3] R. Seshadri and N. A. Hill, Chem. Mater. **13**, 2892 (2001).
[4] N. A. Hill and K. M. Rabe, Phys. Rev. B **59**, 8759 (1999).
[5] B. Ruette, S. Zvyagin, A. P. Pyatakov, A. Bush, J. F. Li, V. I. Belotelov, A. K. Zvezdin, and D. Viehland, Phys. Rev. B **69**, 064114 (2004).
[6] V. Zalesskiĭ, A. A. Frolov, T. A. Khimich, and A. A. Bush, Phys. Solid State **45**, 141 (2003).
[7] F. M. Bai *et al.*, Appl. Phys. Lett. **86**, 032511 (2005).
[8] Y. P. Wang, L. Zhou, M. F. Zhang, X. Y. Chen, J. M. Liu, and Z. G. Liu, Appl. Phys. Lett. **84**, 1731 (2004).
[9] G. L. Yuan, K. Z. Baba-Kishi, J.-M. Liu, S. W. Or, Y. P. Wang, and Z. G. Liu, J. Am. Ceram. Soc. **89**, 3136 (2006).
[10] G. L. Yuan and S. W. Or, J. Appl. Phys. **100**, 024105 (2006).
[11] G. L. Yuan and S. W. Or, Appl. Phys. Lett. **88**, 062905 (2006).
[12] G. L. Yuan, S. W. Or, J. M. Liu, and Z. G. Liu, Appl. Phys. Lett. **89**, 052905 (2006).
[13] R. Haumont, J. Kreisel, P. Bouvier, and F. Hippert, Phys. Rev. B **73**, 132101 (2006).
[14] H. Nadifi, A. Ouali, C. Grigorescu, H. Faqir, O. Monnereau, L. Tortet, G. Vacquier, and C. Boulesteix, Supercond. Sci. Technol. **13**, 1174 (2000).
[15] S. T. Zhang *et al.*, Appl. Phys. Lett. **88**, 1 (2006).
[16] R. E. Melgarejo, M. S. Tomar, R. Guzman, and S. P. Singh, Ferroelectrics **324**, 101 (2005).
[17] M. K. Singh, H. M. Jang, S. Ryu, and M. H. Jo, Appl. Phys. Lett. **88**, 042907 (2006).
[18] M. K. Singh, S. Ryu, and H. M. Jang, Phys. Rev. B **72**, 132101 (2005).
[19] H. J. Yi, M. G. Kim, J. H. Park, and H. M. Jang, J. Appl. Phys. **96**, 5110 (2004).
[20] D. Wu, Y. Deng, C. L. Mak, K. H. Wong, A. D. Li, M. S. Zhang, and N. B. Ming, Appl. Phys. A: Mater. Sci. Process. **80**, 607 (2005).

Downloaded 10 Feb 2009 to 158.132.12.80. Redistribution subject to AIP license or copyright; see http://jap.aip.org/jap/copyright.jsp